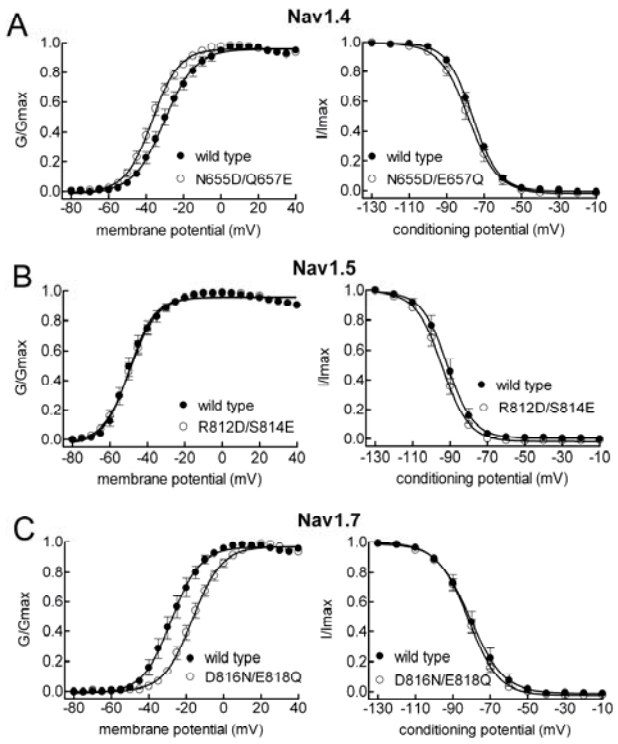

Supplemental Figure 1: Functional properties of activation and inactivation kinetics of WT and double mutant sodium channels expressing HEK293 cells. Channel conductance (G, left column) and steady-state inactivation (right column) were calculated as described in the legend of Figure 3. Cells were held at -100 mV. Recording currents from Nav1.4 (A), Nav1.5 (B) and Nav1.7 (C) started 5 min after establishing whole-cell configuration. Each data point came from 6-12 cells.

Supplemental Table 1

	Nav1.4 WT	Nav1.4 N655D/Q657E	Nav1.5 WT	Nav1.5 R812D/S814E	Nav1.7 WT	Nav1.7 D816N/E818Q
Activation ($V_{1/2}$, mV)	-30.4 ± 0.5	-36.9 ± 0.4	-49.9 ± 0.6	-45.9 ± 0.5	-28.0 ± 0.6	-16.7 ± 0.4
Slope factor	8.4 ± 0.5	7.3 ± 0.4	6.9 ± 0.5	7.4 ± 0.4	7.7 ± 0.5	7.7 ± 0.4
Inactivation ($V_{1/2}$, mV)	-76.1 ± 0.4	-78.3 ± 0.7	-91.5 ± 0.9	-94.3 ± 0.6	-80.9 ± 1.0	-81.7 ± 0.6
Slope factor	7.0 ± 0.3	7.8 ± 0.6	7.0 ± 0.8	7.2 ± 0.5	8.9 ± 0.9	8.0 ± 0.5

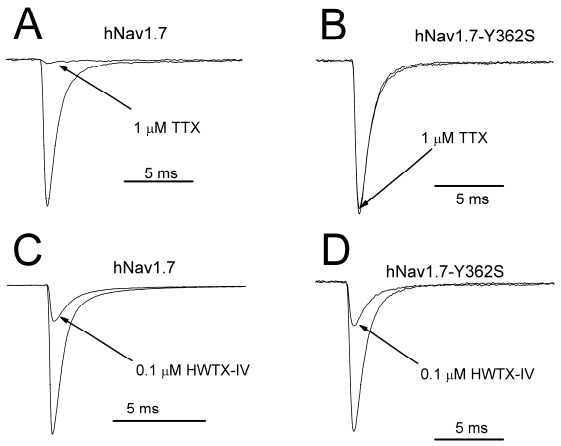

Supplemental Figure 2. A pore mutation that greatly decreases the sensitivity of VGSCs to TTX does not alter the sensitivity of Nav1.7 to HWTX-IV. (A,B) The Y362S mutation, located in the pore loop of domain 1, decreases the sensitivity of sodium channels to TTX by over 1000-fold. HWTX-IV (0.1 μM) inhibits wild-type Nav1.7 channels (C) by 71 ± 3% (n=5) and Nav1.7-Y362S channels (D) by 69 ± 4% (n=4).

```
HwTx-I    ACKGVFDACTPGKNECC--PNRVCSDKHKWCKWKL
HwTx-IV   ECLEIFKACNPSNDQCCKSSKLVCSRKTRWCKYQI
ProTx-II  YCQKWMWTCDSERK-CC--EGMVC—-R-LWCKKKLW
```

Supplemental Figure 3. Alignment of amino-acid sequences for HWTX-I, HWTX-IV and ProTx-II are shown. Residues that are conserved between HWTX-IV and the other two toxins are shaded.